Korean J. Chem. Eng., 37(9), 1541-1551 (2020)
DOI: 10.1007/s11814-020-0523-4

pISSN: 0256-1115
eISSN: 1975-7220

Production of a magnetic biosorbent for removing pharmaceutical impurities

Shokoofeh Fakhrian and Hadi Baseri†

School of Chemistry, Damghan University, Damghan, Iran
(*Received 13 November 2019 • Revised 10 February 2020 • Accepted 27 February 2020*)

Abstract−A magnetic biosorbent was synthesized from rice straw (a biological waste) and magnetic particles of Fe_3O_4. The produced biosorbent, which was characterized by XRD, FE SEM, FTIR, and TGA experiments, was used for adsorption of two drug chemical components of Penicillin G and Amlodipine Besylate from aqueous solutions. Effects of various operating parameters such as adsorption temperature (10 to 70 °C), the dose of adsorbent (1 to 5 g/L), contact time (30 to 360 min), and pH of system (pH=4 to 11) on the adsorption efficiency were studied. The produced adsorbent can remove impurities with maximum adsorption efficiency of about 95% for Pen-G and 65% for AMB; therefore, it is a good adsorbent for removing pharmaceutical impurities from wastewater. Moreover, the produced biosorbent can easily separate from the solution by using an external magnetic field. Five isotherm models--linear adsorption model, Langmuir, Freundlich, Sips, and Toth--were used for describing the results; and based on Langmuir isotherm, the maximum adsorption capacity of the produced biosorbent is 164.7 mg/g for Pen-G and 229 mg/g for AMB. The adsorption kinetics was well fitted with the pseudo-first-order kinetic model, and it is shown that the adsorption is extremely in physical mode.

Keywords: Nano Adsorbent, Penicillin G, Amlodipine Besylate, Fe_3O_4, SiO_2

INTRODUCTION

The increasing rate of waste generation is a major problem in many countries and the demand for environmentally clean products and the companies that can reuse or treat their wastes is growing rapidly. Especially in the chemistry and chemical engineering industries, for minimizing the costs, it is necessary that all the possibilities for reusing their wastes and by-products are studied [1-3]. In addition, production of many useful products with the scarcity of raw materials may improve by treatment and reuse of the wastes [4-6].

Adsorption of industrial pollution for the wastewater treatment is a major demand for various industries. Biosorbents constructed from agricultural wastes such as rice straw or citrus skin have arisen within the last few years [7]. Among them, adsorbents constructed from magnetite and waste materials may have several advantages, which include inexpensive, high adsorption efficiency, high temperature stability, and easier usability over traditional adsorbents such as activated carbons [8,9].

Rice straw is an agricultural waste with more than 580 million tons available worldwide annually [10], but its usage is very limited, and most of the remaining straw after harvest is either burned or left on the ground [11]. Rice straw is mainly used for the production of biofuel, paper [12,13], and especially bio chemicals like bio ethanol or fermentation products [14,15]. Silica content of rice straw is relatively high (10-15%) [16]; therefore, it can be used as a valuable source of bio-nano-silica. Nano silica (SiO_2) has many applications, such as optical fibers, glasses, adsorbents, drug delivery system, and so on [17]. Approximately 10 million tons of silica may be extracted per day from unused rice straw [16].

Silica may be identified as an ideal coating layer for production of adsorbent materials for its several advantages including low-cost, non-toxicity, biocompatibility, high-availability, good porosity, facile surface modification and reaction with other materials [18,19].

Ferrous oxide (Fe_2O_3 and Fe_3O_4) has been widely studied as photocatalyst or absorbent material in water treatment systems [21]. Among them, magnetite (Fe_3O_4) shows strong magnetic effects and, therefore, is widely used for adsorption of impurities from aqueous solutions, because it leads to improve the adsorption efficiency and better separation of adsorbent powder from the solution. For example, the composite of magnetite-activated carbon is used by Akbari and coworkers [21] for adsorption of phenol from aqueous solution. Researchers previously focused on the absorption of various substances such as heavy metal ions [22] or other organic impurities [23] by magnetite. Moreover, many researchers constructed composites of magnetite with organic and inorganic materials and used the produced particles for the treatment of contaminated waters. Among them, SiO_2-Fe_3O_4 composites were produced for removing heavy metals [24] or phosphate [25]. Furthermore, this composite material was used for adsorption of pharmaceutical components like phenanthrene [26], doxorubicin hydrochloride [27], Amitriptyline and Nortriptyline [28].

Antibiotics are one of the famous classes of pharmaceutical compounds used for treatment of bacterial infections in humans and animals. However, about 90% of the used doses may remain undegraded in the environment [29]. Antibiotics have toxic nature toward lower organisms like algae or bacteria, and even at low concentrations they could cause a long-term effect on environment [30]. Antibiotics may lead to bad effects on humans and animals, including chronic toxicity, acute, and emergence of multi-resistant

†To whom correspondence should be addressed.
E-mail: Baseri@du.ac.ir, Hadi.bass@yahoo.com

bacteria [31]. Therefore, due to their release in soil and natural water, the use of antibiotics has drawn major attention of the scientific community.

In this work, a nanocomposite of bio-nano SiO_2-Fe_3O_4 was constructed, and the adsorption of two pharmaceutical components of Penicillin G (Pen-G) and Amlodipine Besylate (AMB) from aqueous solutions were studied. The effects of various effective parameters on the adsorption efficiency were also investigated.

EXPERIMENTAL

1. Materials

All of the chemicals and reagents used were of analytical grade without any further purification (except rice straw sample). Ammonia solution, ferric chloride hexahydrate ($FeCl_3 \cdot 6H_2O$), ferrous sulfate heptahydrate ($FeSO_4 \cdot 7H_2O$), NaOH, HCl, HNO_3, sodium chloride (NaCl) and sulfuric acid (H_2SO_4, 98% pure) were purchased from Merck (Germany). Amlodipine Besylate was collected from Damavand Daroo Co. Damghan, Iran. Penicillin G (potassium-based) was obtained from Aboo Reihan Co. Tehran, Iran. For preparing solutions and in the purification steps, double-distilled deionized water was used. All other chemical compounds were purchased from Merck (Germany). Rice straw was collected from paddy fields of Babol, Iran. And bio-nano-silica powder was extracted from rice straw and utilized for the synthesis of the nano adsorbent composite.

2. Instrumentation

The crystal structure and crystallite size of the produced nano adsorbent were determined by XRD analysis (D8-Advance, Bruker AXS, Cu K α1, λ=1.54 °A). Fourier transform infrared spectrum (Spectrum RXI) was used for determination of the functional groups of synthesized nano adsorbent. The exact size and shape of the nanoparticles were determined by Field emission scanning electron microscopy (HITACHI S-4160). UV-Vis spectroscopy was used for the determination of Pen-G and AMB concentration in aqueous solution (lambda 25). Nanoparticles were separated from the solution by centrifuging in 25 °C (SE.148, Max 6,000 RPM).

3. Synthesis of Nano Magnetite Particles

6.1 g of $FeCl_3 \cdot 6H_2O$ and 4.2 g $FeSO_4 \cdot 7H_2O$ were dissolved in 100 mL of deionized double distilled water with continuous stirring for 1 hour and 100 °C. Then 10 mL of ammonium hydroxide (25%) was added to the system dropwise and mixed for about 30 min. The temperature of the system reduced to 80 °C and maintained for 1 hour and then cooled to room temperature. The dark precipitate was collected by centrifuging and washed three times by water and acetone. Finally, it was dried in 90 °C oven for 5 hours and stored in a closed flask.

4. Synthesis of Bio-nano-silica

At first, for production of bio-nano-silica, 100 g of purified rice straw was washed three times with double distilled water and mixed with 10% sulfuric acid solution in its boiling temperature and for 1 hour in the refluxing mode. Then the straw was washed three times again by double distilled water and dried for 4 hours in 90 °C oven. Finally, the dried straw was calcined for 5 hours in 600 °C and then 4 hours in 900 °C in a muffle furnace. The calcinations were carried out in N_2 atmosphere and the rate of increasing of temperature was 10 °C per min. The remaining white powder was collected and stored in an isolated place for other experiments.

5. Synthesis of Nano Adsorbent Composite

For synthesizing of nano adsorbent, 0.2 g of nano magnetite was dispersed in 40 ml of double-distilled water and mixed at 30 °C for 60 min. Then 0.1 g of synthesized bio-nano silica was added to the mixture in 30 °C and for 60 min. The pH of solution remained constant in pH=6 by using NaOH or HCl solutions (0.1 M). The obtained particles were separated by the magnetic field and centrifuging, and finally washed three times with distilled water and ethanol and dried in 80 °C oven.

6. Procedures

Pen-G and AMB are considered as an antibiotic and non-antibiotic pharmaceutical pollutant in water resources and their efficient removal from wastewater is important. Adsorption tests were carried out for estimation of the adsorption ability of synthesized nano adsorbents. pH values of the solutions were adjusted using NaOH or HCl (0.1 M). In a typical removal procedure, 0.2 g of absorbent nanoparticles was added into 100 mL of Pen-G or AMB contaminated solutions with various concentrations. Then the system was mixed for 3 hours in the desired temperature on a magnetic hitter/stirrer (500 RPM). After mixing, for separating of adsorbent samples from solution, the mixtures were placed under an external magnetic field for about 15 min and centrifuged for 15 min (4,000 RPM). In the supernatant solution, Pen-G/AMB concentration was measured by UV-Vis spectroscopy. The samples were analyzed three times and average values were used in the graphs. In aqueous solution, the concentrations of Pen-G/AMB were scanned in the spectrum mode from the range of 200 to 400 nm, and the overlaid UV spectra were measured [32]. (In order to determine the concentration of solutions, the calibration curves were plotted for each of experimental sets). The following equations were used for calculation of the adsorption efficiency and adsorption capacity:

$$\text{Adsorption efficiency } \% = \frac{(C_0 - C_t)}{C_0} \times 100 \quad (1)$$

$$\text{Adsorption capacity } \left(\frac{\text{mg}}{\text{g}}\right) = \frac{(C_0 - C_t) \times V}{m} \quad (2)$$

where C_0 and C_t are the initial and terminal concentrations of drugs in the solutions, and V and m are the solution volume and weight of adsorbent, respectively.

7. Experimental Design

The effects of six various parameters of initial concentration of drug components in aqueous solution, concentration of nano silica in the adsorbent composite, adsorbent dose, temperature of the solution, pH of the solution and adsorption time on the adsorption efficiency were investigated and optimized by using 26 various experiments. The studied parameters and their levels are reported in Table 1. As can be seen, the effects of each parameter were studied in constant values of other parameters.

RESULT AND DISCUSSION

As can be seen from Fig. 1, the use of magnetite-silica (Fe_3O_4-SiO_2) biosorbent as an adsorbent in water treatment provides a suitable

Table 1. Experimental design for studying the effects of six effective parameters on the adsorption efficiency of pharmaceutical components

No.	In. con.	Si. con.	Dos. ads.	Tem.	pH	Time
	ppm	W%	g/L	K		min
1	50	33	3	313	8	180
2	67	33	3	313	8	180
3	84	33	3	313	8	180
4	100	33	3	313	8	180
5	118	33	3	313	8	180
6	84	20	3	313	8	180
7	84	33	3	313	8	180
8	84	50	3	313	8	180
9	84	60	3	313	8	180
10	84	33	1	313	8	180
11	84	33	2	313	8	180
12	84	33	3	313	8	180
13	84	33	5	313	8	180
14	84	33	3	283	8	180
15	84	33	3	303	8	180
16	84	33	3	323	8	180
17	84	33	3	343	8	180
18	84	33	3	313	4	180
19	84	33	3	313	6	180
20	84	33	3	313	7	180
21	84	33	3	313	9	180
22	84	33	3	313	11	180
23	84	33	3	313	8	30
24	84	33	3	313	8	120
25	84	33	3	313	8	240
26	84	33	3	313	8	360

Fig. 1. Magnetic nature of produced biosorbent.

and comfortable approach for separating the pollutants by applying the external magnetic fields.

1. Characterization of Nano Adsorbents

The crystalline structures and crystallite size of synthesized nano adsorbent are recognized with XRD patterns (Fig. 2). The peaks with 2θ values of 35.5°, 43.3°, 57.2°, and 62.8° in Fig. 2(a) were observed for nano magnetite in the spinal cubic form. For Fig. 2(b), the peaks with 2θ values of 21.8, 36, 42.5, and 46.8 confirmed the octagonal crystal shape of silica without any impurities. The XRD pattern of magnetite-silica nanocomposite is reported in Fig. 2(c). Peaks at 2θ values of 30, 35.4, 43, and 65.2 show that the cubic form of magnetite remained constant with a coating of silica molecules. This XRD pattern agrees with other works [33]. The average crystallite size of the produced adsorbent was calculated by using Scherrer's formula (3) [34]:

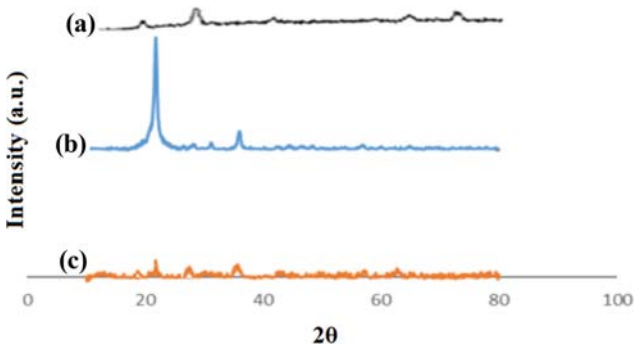

Fig. 2. XRD patterns of (a) pure magnetite, (b) bio SiO_2 and (c) nano composite of SiO_2-magnetite.

Table 2. Crystallite size of synthesized samples

Nano particle	Crystallite size (nm)
SiO_2	25
Fe_3O_4	16
SiO_2-Fe_3O_4	31

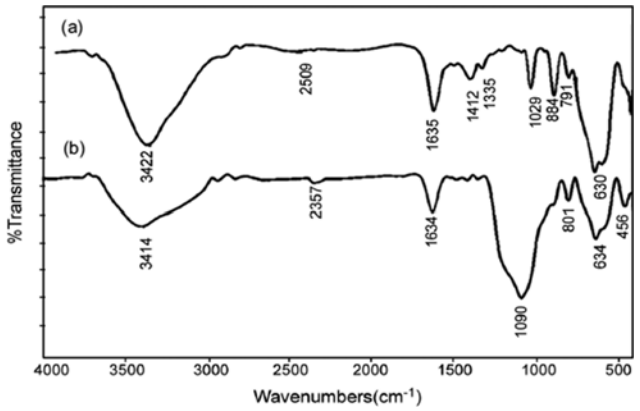

Fig. 3. FT-IR spectra of nano (a) Fe_3O_4 and (b) SiO_2-Fe_3O_4 nano adsorbent.

$$D = \frac{K\lambda}{\beta \cos\theta} \quad (3)$$

where D is the average crystallite size, K is a constant equal to 0.9, λ is 1.5406 A°, θ is Bragg angle for the diffraction peaks, and β is the full width at half maximum (FWHM) in radians on the 2θ scale. The calculated results are reported in Table 2.

The FT-IR of magnetite and magnetite-silica composite is shown

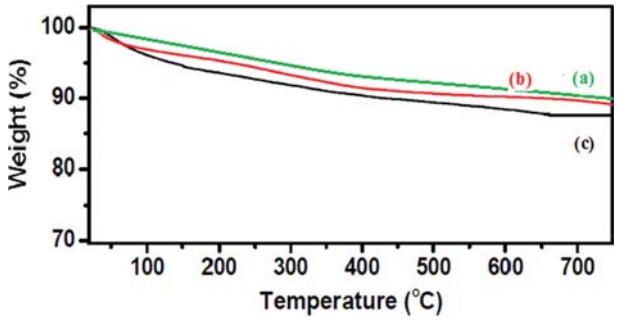

Fig. 4. Thermogravity analyses diagram of (a) pure silica, (b) magnetite, and (c) magnetite-silica nano adsorbent.

in Fig. 3. The major peaks at 568 and 630 cm^{-1} appearing in the FT-IR spectrum are related to Fe-O vibration bands. The peaks of about 3,000 to 3,500 cm^{-1} are due to the normal polymeric O-H stretching vibrations of H_2O molecules that may physically adsorb in the surface of nanoparticles. For the IR spectrum of magnetite-silica, the peak at about 1,090 cm^{-1} is related to Si-O bonds, and a peak of about 634 cm^{-1} shows the Si-O-Fe vibration bands. Adsorption bonds in 989 and 801 cm^{-1} are related to Si-OH and Si-O-Fe structures, which agrees with other works [35].

The thermogravimetric analysis of silica, magnetite and SiO_2-magnetite in the N_2 atmosphere at a heating rate of 10 °C/min is shown in Fig 4; the reduction of weight in temperatures below 250 °C (below 10%) is attributed to the release of water incorporated in the raw sample. The second weight loss from 250 to 700 °C may be due to the degradation of Fe-O bonds in Fe_3O_4 molecules [36].

FE-SEM images of produced nano biosilica, nano Fe_3O_4 and composite of nano biosilica-nano Fe_3O_4 are shown in Fig. 5. Based on the reported results, in the all samples agglomerated nanoparticles were formed. Because, nano silica particles have surface charges and in both other samples, Fe_3O_4 has super magnetic effects, and it caused the agglomeration of particles. The histogram of particle size distribution is presented in Fig. 6. As can be seen, the mean sizes of the produced particles are about 60 nm. For pure magnetite samples, larger agglomerated particles are formed. But, in SiO_2-Fe_3O_4 particles, silica may cause lower agglomeration effects.

2. Effects of Various Parameters on the Adsorption Efficiency

The adsorption of Pen-G and AMB in the aqueous solution was studied by using the produced nano biosorbent, and the effects of six various effective parameters on the adsorption efficiency were demonstrated.

2-1. Effect of Initial Concentration

The effects of initial concentration of a drug on the adsorption efficiency were studied in the five values of (50, 67, 84, 100, and 118 ppm for Pen-G and 61, 82, 102, 123, and 143 ppm for AMB). The effect of various concentration of Pen-G on the adsorption efficiency and adsorption capacity (mg/g) for pure nano magnetite and nano silica-magnetite composite particles are reported in Fig. 7. As can be seen, by increasing of Pen-G concentration in aqueous solution from 50 to 84 ppm, the adsorption efficiency is in-

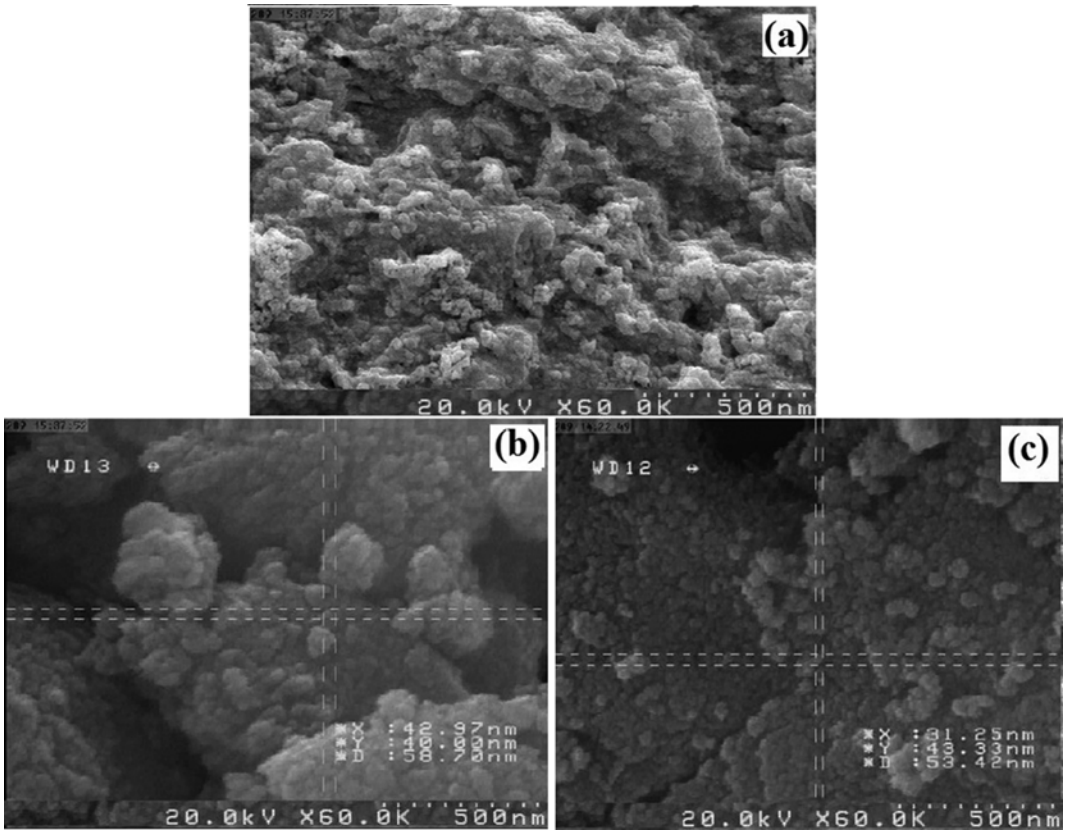

Fig. 5. FE-SEM image of (a) pure silica, (b) magnetite, and (c) magnetite-silica nano adsorbent.

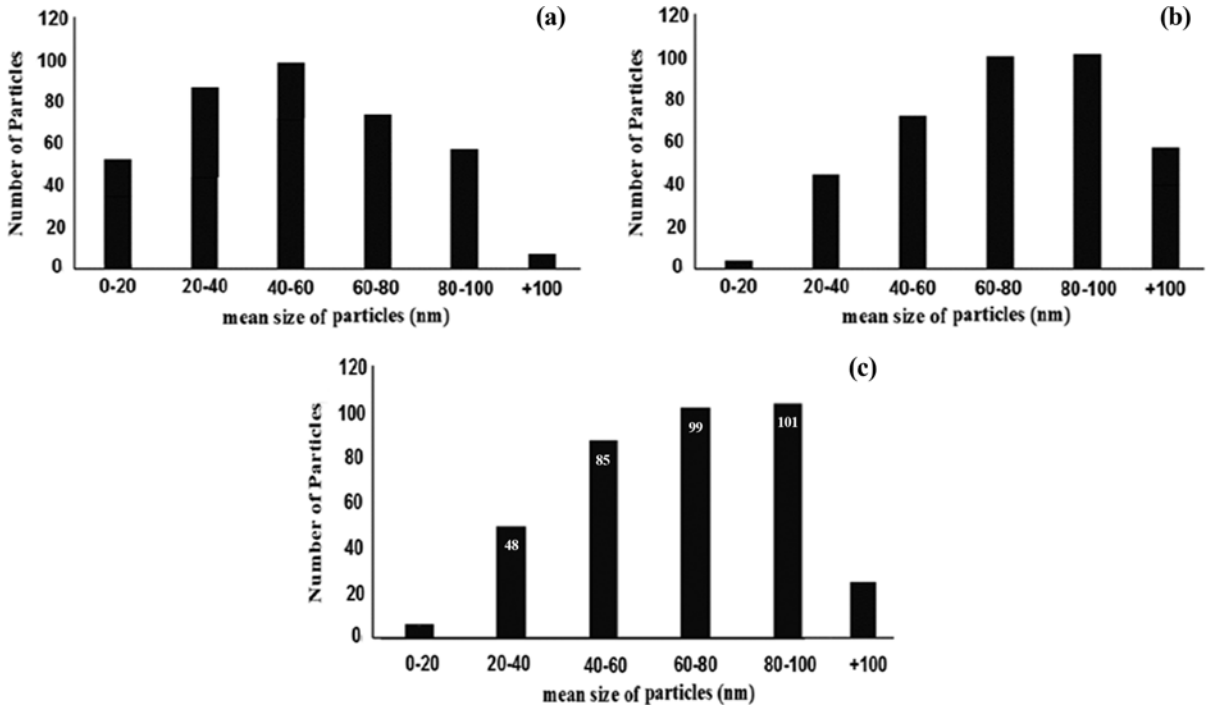

Fig. 6. Obtained Histogram from FE-SEM images of (a) pure silica, (b) magnetite, and (c) magnetite-silica nano adsorbent.

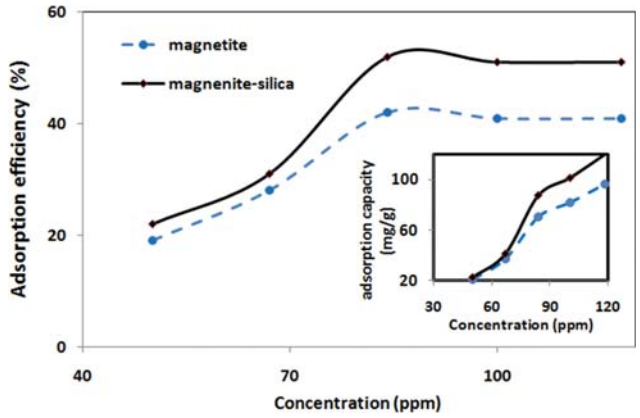

Fig. 7. Effects of various concentrations of Pen-G on the adsorption efficiency and adsorption capacity for pure magnetite and magnetite-silica nano adsorbent.

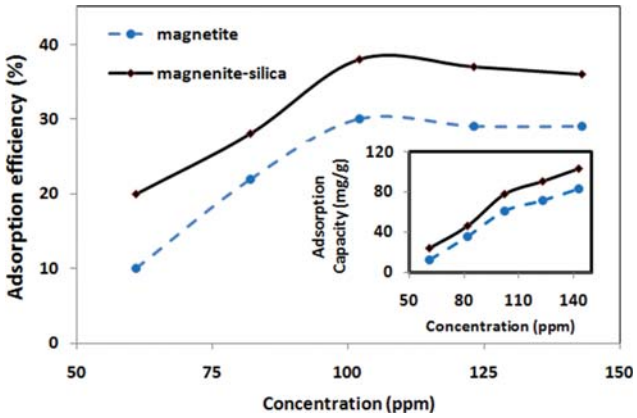

Fig. 8. Effects of various concentrations of AMB on the adsorption efficiency and adsorption capacity for pure magnetite and magnetite-silica nano adsorbent.

creased from 20 to 50%, but by further increase of drug concentration until 118 ppm the adsorption efficiency relatively remained constant. This effect may be attributed to the saturation of adsorption sites in the adsorbent particles. Moreover, based on the reported results, the magnetite-silica nanocomposite shows better adsorption efficiency in all examined concentrations, and especially at higher concentrations, the adsorption efficiency of the produced nano adsorbent composite is 10% higher than pure magnetite. Moreover, in all studied concentrations by increasing the Pen-G concentration the adsorption capacity increased also.

Relatively same results were reported by Nourmoradi and coworkers [37], in which the adsorption of Pen-G increased by increasing the initial concentration of Pen-G in concentration ranges below 150 mg/L (ppm) with mineral clay as adsorbent. But based on the reported results of Ghamkhari and coworkers [37], the adsorption of Pen-G decreased by increasing the initial concentration in concentration values of about 10 mg/L for the polymer-Fe_3O_4 composite adsorbent.

Fig. 8 shows the effect of AMB concentration on the adsorption efficiency and adsorption capacity for pure nano magnetite and nano silica-magnetite composite particles. Based on the results of this figure, in aqueous solution, an increase of AMB concentration from 61 to 102 ppm leads to an increase of adsorption efficiency from 20 to 50%, but by more increasing of drug concentration until 143 ppm the adsorption efficiency relatively remains constant. Moreover, the adsorption efficiency of magnetite-silica nanocomposite is relatively 10% higher in all concentrations. Specifically in low con-

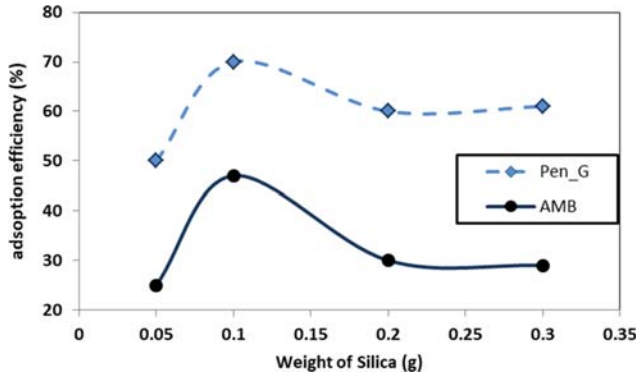

Fig. 9. Effects of silica content in the produced magnetite-silica adsorbent on its adsorbent efficiency (pH=8, 0.3 g dose of adsorbent, temperature of 313 K, and adsorption time of 180 min).

centrations, the magnetite-silica adsorbent shows removal efficiency extremely better than the pure magnetite (about 100%).

2-2. Effect of Various Concentrations of Silica in the Adsorption efficiency of the Produced Biosorbent

The concentration of silica in the silica-magnetite nanocomposite is an efficient parameter for the adsorption of drug compounds. In Fig. 9, different values of silica (0.05 to 0.3 g) are used for the production of nano adsorption composite by mixing with the constant weight of magnetite (0.2 g). Different types of produced adsorbents adsorbed the drug compounds with different efficiencies. The results show that the composite of 0.1 g nano silica with 0.2 g magnetite has maximum adsorption efficiency for both studied drugs. Therefore, this value was used for all other experiments.

Nano silica particles are suitable adsorbents [39] and increase of nano-silica must increase the adsorption power of produced adsorbent by increasing the adsorption sites. Moreover, addition of silica leads to increase of the porosity of produced composite [18,19]. But increase of silica weight percent in the mixture of silica-magnetite may lead to increase the coating effect of silica on the surface of magnetite, and therefore increase of silica weight percent may decrease the adsorption effect of magnetite. It also leads to decrease of the adsorption power of adsorbent composite. As can be seen from Fig. 9, the optimum concentration of SiO_2 for maximum adsorption of Pen-G and AMB is 0.1 g SiO_2 in 0.2 g of magnetite.

Zhao and coworkers [40] reported the same results for adsorption of Tetracycline from the aqueous solutions. They show that silica addition greatly enhanced the adsorption capacity of bamboo produced biochar in concentrations below 30% w.

2-3. Effect of Various Dose of Adsorbent in the Adsorption Efficiency

Fig. 10 shows the effect of adsorbent dose (weight/volume of solution) on the adsorption efficiency of Pen-G and AMB from the aqueous solution. This figure shows that by increasing of adsorbent dose, the adsorption efficiency increased. But in adsorbent doses higher than 3 g/L, the increasing slopes of curves decreased, and therefore, 3 g/L of adsorbent was selected for all other experiments.

As mentioned by Ghorbani and coworkers [18], by increasing of the sorbent dosage the removal efficiency increased. Because, the number of adsorption sites increased. However, at higher sorbent dosages the access to active sites with relatively high-energies decrease. This results in decreased adsorption capacity. Furthermore, by increasing the sorbent dosage the chance of collision among sorbent nanoparticles improves, and particle aggregation increased; therefore, the total surface area decreased, which may cause the reduction of sorbent adsorption capacity.

2-4. Effect of Temperature on the Adsorption Efficiency

The effect of temperature on the adsorption efficiency of Pen-G and AMB is shown in Fig. 11. As can be seen, by increasing temperature from 10 to 40 °C, the adsorption efficiency increased, but by increase from 40 to 70 °C, adsorption efficiency decreased. Probably, decrease of the removal efficiency of drug components with temperature is due to the weakening of adsorptive forces between the active sites of adsorbed molecules and the adsorbate species on the surfaces of nano adsorbents [41,42].

Based on the results of Aksu and coworkers [43], temperature significantly influenced the adsorption of Pen G in higher concentrations. As mentioned by them, 35 °C is the best temperature for adsorption of Pen G by activated carbon.

2-5. Effect of pH of Solution on the Adsorption Efficiency

For determining the speciation of drug components in the solu-

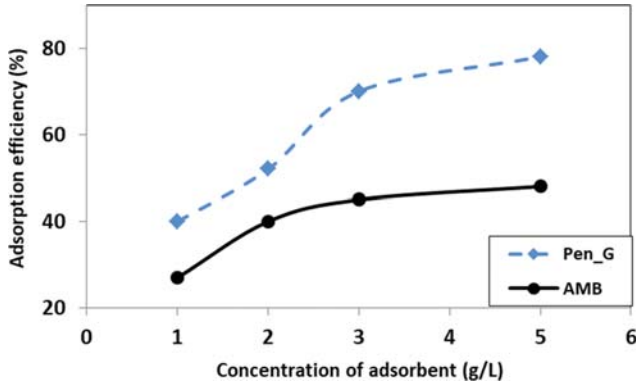

Fig. 10. Effect of adsorbent weight on the adsorption efficiency of Pen-G and AMB by magnetite-silica adsorbent (pH=8, 33% silica content, temperature of 313 K, and adsorption time of 180 min).

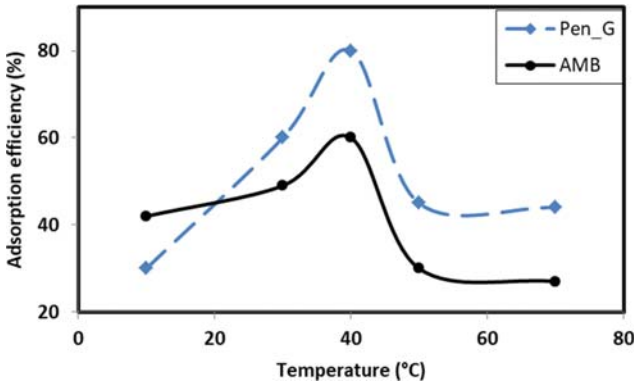

Fig. 11. Effects of solution temperature on the adsorption efficiency of Pen-G and AMB by magnetite-silica adsorbent (pH=8, 33% silica content, 0.3 g dose of adsorbent, and adsorption time of 180 min).

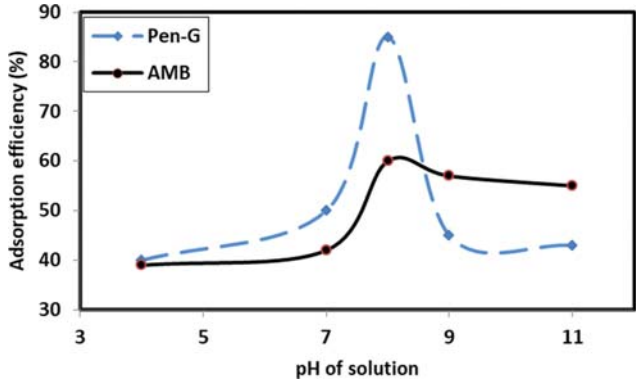

Fig. 12. Effects of the pH of solution on the adsorption efficiency of Pen-G and AMB by magnetite-silica adsorbent (temperature of 313 K, 33% silica content, 0.3 g dose of adsorbent, and adsorption time of 180 min).

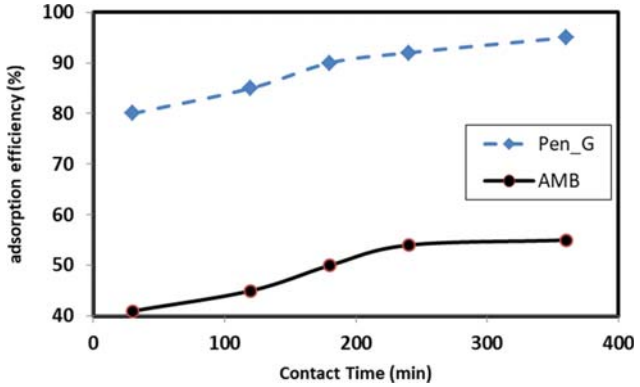

Fig. 13. Effects of contact time on the adsorption efficiency of Pen-G and AMB by magnetite-silica adsorbent (pH=8, temperature of 313 K, 33% silica content, and 0.3 g dose of adsorbent).

tions and for determining the charge on the surfaces of the synthesized adsorbents by their functional groups, pH studies are very important in adsorption processes [44].

The effect of pH of solution on the adsorption of Pen-G and AMB is explained in Fig. 12. It was observed that adsorption and removal of drug components increased with increases in pH of the solution from pH=4 to pH=8 and further decreases or even being constant at the higher pH until pH=11.

By increasing the pH of solution, the deprotonation of acidic functional groups reinforces, and the attraction forces between nano adsorbent and active sites of drug components increase. At pH values higher than 8, the dominance of OH^- ions in the aqueous solution creates a competition between OH^- ions and negatively charged nano adsorbent surface, which resulted in a decrease in the adsorption of drug molecules [45].

As mentioned by Ghamkhari and coworkers [38], the optimum value of pH for maximum adsorption efficiency is related to initial concentration of Pen-G, dose of adsorbent and characteristics of the used adsorbent. For a polymer-Fe_3O_4 composite adsorbent and in 50 mg/L of Pen-G solution concentration, the optimum pH of solution is about 11.

2-6. Adsorption Kinetic Studies

Fig. 13 shows the effect of contact time on the adsorption of Pen-G and AMB at a different times of 30 to 360 min. Based on the reported results of this figure, the constructed nano-biosorbent is a good adsorbent, and specifically for Pen-G, it can remove drug components with efficiencies higher than 90%. Because of the high number of available active sites on the surface of the sorbent materials, the initial rate of removal is high, which results in increased rapid adsorption.

For two studied components, the adsorption efficiency increased by increasing contact time to 360 min, but for Pen-G in times higher than 180 min and for AMB in contact time higher than 240 min, the removal efficiency was relatively constant. Because, after these times, adsorptive sites of produced nano adsorbents were blocked. The contact time of 180 min was selected as an optimum adsorption time. Three kinetic models of pseudo-first-order (PF), pseudo-second-order (PS), and intraparticle diffusion (ID) models were utilized in the rate-determining step. The equations for the models are in Table 3.

For understanding the adsorption process, the three studied models were fitted to the reported experimental data obtained from batch experiments and the R^2 values determined by using non-linear regression analysis. The obtained results are presented in Table 3 and Fig. 14. The R^2 value of the ID and PF kinetic models is higher than the PS models, and the experimental q_e values from the ID and PF models are much closer to the calculated q_e values in comparison with PS model. Therefore, the ID and PS models better describe the adsorption behavior of pharmaceutical components on the magnetic adsorbent. In Fig. 13, the plot of the intraparticle diffusion model demonstrates multilinearity during relatively all the studied time range, and it implies two more steps of the film diffusion and intraparticle diffusion in adsorption process.

Plots of the PF model are shown in Fig. 14. As mentioned later, in comparison to the PS model the PF kinetic model better represents the kinetic data by considering its R^2 value.

3. Adsorption Isotherms

At a constant temperature, the release or retention of a substance

Table 3. Kinetic parameters for adsorption of Pen G and AMB pharmaceutical components

	Pen G			AMB			Equation
	Q	K_i	R^2	Q	K_i	R^2	
Fir. order	350.66^{β}	0.0042^{α}	0.94	361.33^{β}	0.0036^{α}	0.95	$q_t=Q(1-e^{-K_1t})$
Sec. order	211.10^{σ}	0.000165^{γ}	0.82	199.1^{σ}	0.000165^{γ}	0.80	$q_t=K_2Q^2t/(1+K_iQt)$
In. par. dif.	1.1	14.29^{ρ}	0.982	1.1	13.74^{ρ}	0.985	$q_t=K_it^{1/2}+Q$

α: 1/min β: mmol/g γ: g/(mmol min) σ: mmol/g ρ: mg $\sqrt{}$min/g

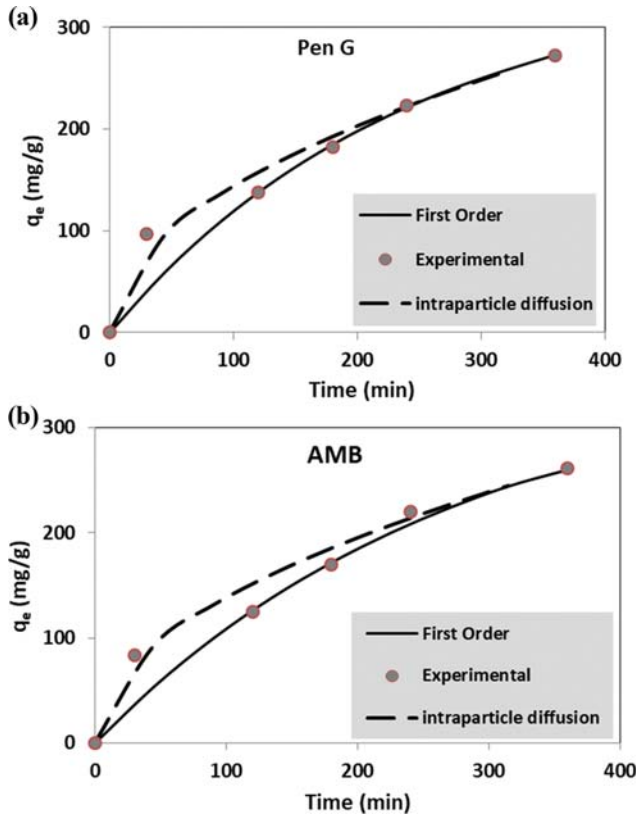

Fig. 14. AMB and Pen-G adsorption kinetics study for pseudo-first-order and intraparticle diffusion model.

from the aqueous phase to a solid phase is described by adsorption isotherm. And they are important in understanding the surface properties, adsorption mechanism, adsorption capacity, as well as adsorbate-adsorbent interactions. For the mathematical description of adsorption isotherms, many different equations are described in the literature [46,47]. In this work, to evaluate the appropriate model describing absorption data, five isotherm models, including one-parameter, two-parameter isotherm models namely Freundlich and Langmuir, and three parameter isotherm models of Sips and Toth isotherm models were used, and the fitting ability of the models wass compared based on their variances.

Linear adsorption model is the simplest adsorption isotherm in which the amount of surface adsorbate is linearly proportional to the partial concentration of the adsorbate.

$$q_e = K_H C_e \tag{4}$$

where q_e is the adsorbate amount at equilibrium (mg/g), K_H is the adsorption constant, and C_e is the concentration of adsorbate on the adsorbent at equilibrium condition.

Langmuir isotherm is the second studied model. In this theory, it is assumed that the coverage of adsorbate over a homogeneous adsorbent surface is monolayer.

$$q_e = \frac{q_{max} K_L C_e}{1 + K_L C_e} \tag{5}$$

where C_e is the surface concentration of adsorbate in equilibrium (mg/L), K_L (L/mg) is the Langmuir constant, and q_m (mg/g) is the maximum adsorption capacity.

The third studied model, the Freundlich isotherm, is an empirical equation that describes the adsorption of molecules on heterogeneous surfaces of the adsorbent.

$$q_e = K_F C_e^{1/n} \tag{6}$$

K_F is the Freundlich constant ((L/mg)$^{1/n}$ (mg/g)) and n is the heterogeneity factor.

Sips (Langmuir-Freundlich) isotherm is the fourth studied model; it is a combination of the Freundlich and Langmuir isotherms.

$$\frac{q_e}{q_m} = \frac{K_S C_e^{\beta_S}}{1 - K_S C_e^{\beta_S}} \tag{7}$$

In this equation, q_m is the Sips isotherm model constant (mg/g), β_S is the Sips isotherm exponent, and K_S is the Sips constant (L/g). The heterogeneity factor of β_S is the difference between the Langmuir and the Sips equations, and usually β_S is lower than 1. Moreover, the smaller is the value of this parameter, the more heterogeneous is the adsorbent surface.

The last studied model is Toth isotherm. Another modification of the Langmuir isotherm is the Toth isotherm, and it is applied for heterogeneous adsorption. In this model, it is considered that most sites have adsorption energy lower than the maximum.

$$\frac{q_e}{q_m} = \frac{K_e C_e}{[1 + (K_e C_e)^n]^{1/n}} \tag{8}$$

where q_m is the constant related to maximum adsorption capacity, K_e is Toth isotherm constant (L/mg). n is the heterogeneity factor, $0 < n \leq 1$. For a homogeneous surface, n=1 and the Toth equation reduces to the Langmuir equation.

As can be seen in Fig. 15, it is evident that almost all the simulation plots of these models fitted well with the experimental data except for linear adsorption model; but by comparison between these models, experimental values are relatively in good agreement with the predicted values of the Sips isotherm. Moreover, based on the results shown in Table 4, R^2 values show linear relationship between Sips model predicted and experimental values. Sips isotherm is a three-parameter model that predicts the mechanism for heterogeneous adsorption systems [48]. At low concentration of adsorbate (β_s=0), the equation follows Freundlich adsorption [48], while At high values of adsorbate concentration (β_s=1), the equation follows Langmuir's monolayer adsorption model. Based on the reported results of Table 4, Magnetite-SiO_2 is a better absorbent of pharmaceutical components in comparison with pure magnetite. For Langmuir isotherm, maximum adsorption capacity (q_m) of magnetite-SiO_2 nano adsorbent is about 164 for Pen-G and 229 for AMB, but these values are about 130 and 171 for pure Magnetite. Moreover, the relatively same results were observed for q_m of the Sips model.

Based on the reported results of Fig. 15 and Table 4, the adsorption of AMB and Pen G at all examined conditions is likely to take place by the formation of multi-layer coverage on the energetically heterogeneous surface of adsorbent [49].

The maximum adsorption capacity (q_m) of Pen-G from aqueous solutions published by previous studies using various adsorbents

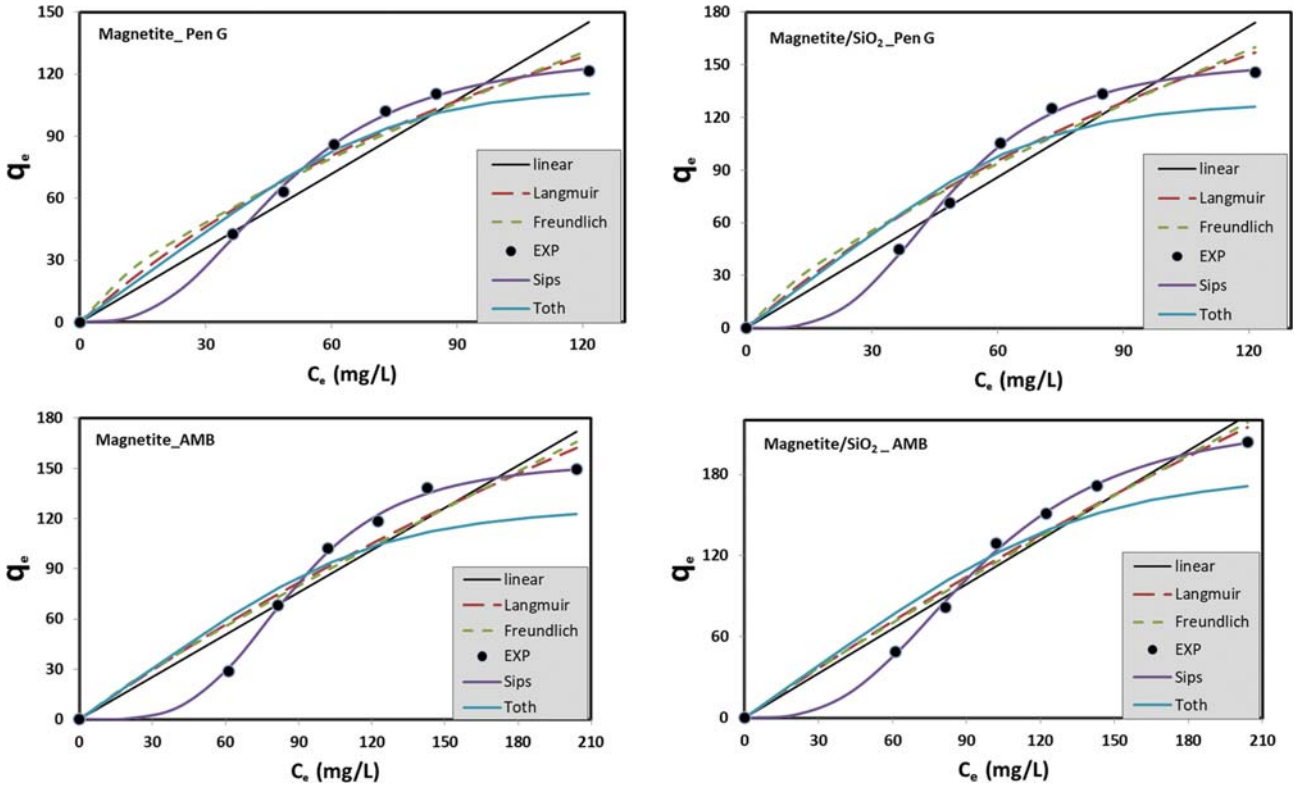

Fig. 15. AMB and Pen-G adsorption isotherms for nano magnetite and nano magnetite SiO_2 adsorption.

Table 4. Parameters of the isotherm models for adsorption of Pen-G and AMB on the Magnetite and Magnetite-SiO_2 nano absorbent

Isotherm	Parameter	Magnetite Pen-G	Magnetite_SiO_2 Pen-G	Magnetite AMB	Magnetite_SiO_2 AMB
Linear	K (L/g)	1.195	1.4318	0.8427	1.0982
	R^2	**0.9098**	**0.9074**	**0.9323**	**0.95**
Langmuir	K_L (L/mg)	4.1769	0.0048	0.0014	0.0009453
	q_m (mg/g)	130.56	164.69	171.30	229.1
	R^2	**0.9606**	**0.9530**	**0.949**	**0.9639**
Freundlich	K_f $(L/mg)^{1/n}$ mg/g	4.1769	4.1952	1.4362	1.5811
	n	1.3913	1.3183	1.1199	1.079
	R^2	**0.9518**	**0.9429**	**0.9393**	**0.9582**
Sips	K_S (L/g)	0.00001573	0.00000194	0.0000000283	0.000000119
	q_m (mg/g)	131.57	153.788	154.71	224.25
	β_S	0.3508	0.2956	0.2547	0.334
	R^2	**0.9993**	**0.9992**	**0.9989**	**1**
Toth	K_e (L/mg)	0.000000006759	0.0000000349	0.00000002092	0.00000002566
	q_m (mg/g)	114.3	130.02	128.13	184.33
	1/n	4.314	4.005	3.652	3.5206
	R^2	**0.9544**	**0.9257**	**0.9037**	**0.9273**

is listed in Table 5. Maximum adsorption capacity was calculated based on Langmuir equation. In each of adsorption experiments, six-hour adsorption time was spent to reach equilibrium and equilibrium concentration (C_e) was measured. Then by using Eq. (2) the equilibrium adsorption capacity (q_e) was calculated. The obtained results were fitted to Langmuir equation and q_m was estimated.

Maximum adsorption capacity may be affected by some parameters such as adsorption temperature, studied range of concentration, and specifically the nature of the adsorbent used. For example, as mentioned by Aksu and Tunç [43], increase of the concentration of Pen-G from about 100 to 1,000 ppm may lead to slightly increase of maximum adsorption capacity.

The comparison between the various adsorbents in Table 5 shows that the SiO_2-Fe_3O_4 is a relatively good adsorbent for removing the

Table 5. Comparison of various adsorbents for adsorptive removal of Pen-G

	Pharmaceutical	Adsorbent	Max ini. con. (ppm)	q_m (mg/g)	References
1	Pen-G	Activated sludge	1,000	330	[43]
2	Pen-G	Activated carbon	1,000	375	[43]
3	Pen-G	Activated sludge	100	75	[43]
4	Pen-G	Activated carbon	100	82	[43]
5	Pen-G	Chestnut Shell	100	100	[50]
6	Pen-G	Modified clay	200	88.5	[37]
7	Pen-G	Fe_3O_4	120	130	This work
8	Pen-G	SiO_2-Fe_3O_4	120	164.7	This work

Pen-G from aqueous solutions.

CONCLUSION

Nanocomposite of SiO_2-Fe_3O_4 was constructed from rice straw, and adsorption of pharmaceutical components of Pen-G and AMB by the produced adsorbent composite were studied. The effects of different parameters of silica content in the produced nano adsorbent, adsorption temperature, the dose of adsorbent, initial concentration of drug components in the aqueous solution, pH of solutions, and contact time on the adsorption efficiency were studied. Based on the reported results in this work, the higher weight of adsorbent and higher contact time lead to higher adsorption efficiency, but other studied parameters show optimum values of 40 °C solution temperature, pH=8, relatively 33% silica content in the adsorbent composite and initial concentrations higher than 200 ppm. The produced magnetic biosorbent can remove pharmaceutical impurities with acceptable efficiency of about 95% for Pen-G and 65% for AMB.

The composite biosorbent of SiO_2-Fe_2O_3 shows relatively 30% better adsorption efficiency in comparison to pure Fe_2O_3. Moreover, this biosorbent shows advantages such as low cost, eco-friendly, easy separation, and higher thermal efficiency.

REFERENCES

1. M. E. Bautista, L. Pérez, M. T. García, S. Cuadros and A. Marsal, *Chem. Eng. J.*, **262**, 399 (2015).
2. G. S. dos Reis, M. Wilhelm, T. C. A. Silva, K. Rezwan, C. H. Sampaio, E. C. Lima and S. M. A. G. U. Souza, *Appl. Therm. Eng.*, **93**, 590 (2016).
3. J. A. Cusidó, L. V. Cremades, C. Soriano and M. Devant, *Appl. Clay Sci.*, **108**, 191 (2015).
4. H. Li, Z. Sun, L. Zhang, Y. Tian, G. Cui and S. Yan, *Colloids Surf. A*, **489**, 191 (2016).
5. U. Moral and S. Sensöz, *Fuel*, **150**, 672 (2015).
6. D. Vamvuka, S. Sfakiotakis and S. Saxioni, *Fuel*, **147**, 170 (2015).
7. R. Kandanlou, M. Bin Ahmad, K. Shameli and K. Kalantari, *Bio Resource*, **9**, 642 (2013).
8. P. Kumar, S. Kumar and L. Joshi, *Socioeconomic and environmental implications of agricultural residue burning: A case study of punjab, India*, Springer Briefs in Environmental Science, Germany, 144 (2015).
9. K. Minu, K. K. Jiby and V. V. N. Kishore, *Biomass Bioener.*, **39**, 210 (2012).
10. S. M. Jani and I. Rushdan, *J. Trop. Agric. and Fd. Sc.*, **44**, 103 (2016).
11. I. Kim, B. Lee, J. Y. Park, S. A. Choi and J. I. Han, *Carbohydr. Polym.*, **99**, 563 (2014).
12. C. F. L. e Silva, M. A. Schirmer, R. N. Maeda, C. A. Barcelos and N. Pereira Jr., *Electron. J. Biotechnol.*, **18**, 10 (2015).
13. P. J. M. Suhas and M. M. L. Ribeiro Carrot, *Bioresour. Technol.*, **98**, 2301 (2007).
14. S. H. Ghaffar and M. Fan, *Int. J. Adhes.*, **48**, 92 (2014).
15. A. Abraham, A. K. Mathew, R. Sindhu, A. Pandey and P. Binod, *Bioresour. Technol.*, **215**, 29 (2016).
16. H. Baseri and S. Tizro, *Process Saf. Environ. Prot.*, **109**, 465 (2017).
17. W. Guan, X. Gao, G. Ji, Y. Xing, C. Du and Z. Liu, *J. Solid State Chem.*, **255**, 150 (2017).
18. F. Ghorbani and S. Kamari, *Environ. Technol. Innovation*, **14**, 100333 (2019).
19. A. Kamgar, S. Hassanajili and G. Karimipourfard, *J. Environ. Chem. Eng.*, **6**, 3034 (2018).
20. Q. Yuan, N. Y. Chi, W. Geng, W. Yan, Y. Zhao, X. Li and B. Dong, *J. Hazard. Mater.*, **255**, 157 (2013).
21. Z. A. Jonoush, M. Farzadkia, Y. D. Shahamat and A. E. dizaji, *J. Mazandaran Univ. Med. Sci.*, **25**(122), 158 (2015).
22. H. Ding, Y. Zhao, Q. Duan, J. Wang, K. Zhang, G. Ding, X. Xie and C. Ding, *J. Rare Earths*, **35**(10), 984 (2017).
23. B. MirzaHedayata, M. Noorisepehr, E. Dehghanifard, A. Esrafili and R. Norozi, *J. Mol. Liq.*, **264**(15), 571 (2018).
24. H. R. Pouretedal and N. Sadegh, *J. Water Process Eng.*, **1**, 64 (2014).
25. M. R. Samarghandi, T. J. Al-Musawi, A. Mohseni-Bandpi and M. Zarrabi, *J. Mol. Liq.*, **211**, 431 (2015).
26. L. Wang, C. Shen and Y. Cao, *J. Phys. Chem. Solids*, **116**, 72 (2018).
27. W. Caia, M. Guo, X. Weng, W. Zhang and Z. Chen, *Mater. Sci. Eng. C*, **98**, 65 (2019).
28. B. Fahimirad, M. Rajabi and A. Elhampour, *Anal. Chim. Acta*, **275**, 1047 (2019).
29. E. Alizadeh and H. Baseri, *Solid State Sci.*, **78**, 86 (2018).
30. Q. Y. Li, K. R. Ma, Z. J. Ma, Q. Wei, J. G. Liu, S. P. Cui and Z. R. Nie, *Micropor. Mesopor. Mater.*, **265**, 18 (2018).
31. B. D. Cullity and S. R. Stock. *Elements of X-ray diffraction*, 3rd Ed. Prentice Hall, New York (2001).
32. R. Wang, X. Wang, X. Xi, R. Hu and G. Jiang, *Adv. Mater. Sci. Eng.*, **2012**, 1 (2012).
33. C. M. Babu, B. Palanisamy, B. Sundaravel, M. Palanichamy and V.

Murugesan, *J. Nanosci. Nanotechnol.*, **13**(4), 2517 (2013).
34. M. Hu, X. Yan, X. Hu, J. Zhang, R. Feng and M. Zhou, *J. Colloid Interface Sci.*, **510**, 111 (2018).
35. M. Ahmaruzzaman and S. L. Gayatri, *Chem. Eng. Data J.*, **55**, 4614 (2010).
36. A. E. Ofomaja and Y. S. Ho, *Dyes Pigm.*, **74**, 60 (2007).
37. H. Nourmoradi, A. Daneshfar, S. Mazloomi, J. Bagheri and S. Barati, *Methods X*, **6**, 1967 (2019).
38. A. Ghamkhari, L. Mohamadi, S. Kazemzadeh, M. N. Zafar, A. Rahdar and R. Khaksefidi, *Composites Part B*, **182**, 5 (2020).
39. M. Ahmaruzzaman and V. K. Gupta, *Ind. Eng. Chem. Res. J.*, **50**, 13589 (2011).
40. Z. Zhao, T. Nie and W. Zhou, *Environ. Pollut.*, **254**, 113015 (2019).
41. S. M. de Oliveira Brito, H. M. C. Andrade, L. F. Soares and R. P. de Azevedo, *J. Hazard. Mater.*, **174**, 84 (2010).
42. N. Ayawei, A. N. Ebelegi and D. Wankasi, *J. Chem.*, **2017**, 11 (2017).
43. Z. Aksu and Ö. Tunç, *Process Biochem.*, **40**, 831 (2005).
44. J. Sreńscek-Nazzal, U. Narkiewicz, A. W. Morawski and R. J. Wróbel, *J. Chem. Eng. Data*, **60**, 3148 (2015).
45. J. Srenscek-Nazzal, U. Narkiewicz, A. W. Morawski, R. J. Wrobel and B. Michalkiewicz, *J. Chem. Eng. Data*, **60**, 3148 (2015).
46. K. W. Jung, S. Y. Lee and Y. J. Lee, *Bioresour. Technol.*, **261**, 1 (2018).
47. N. A. H. M. Zaidi, L. B. L. Lim and A. Usman, *Environ. Technol. Innovation*, **13**, 211 (2019).
48. V. Nejadshafiee and M. RezaIslami, *Mater. Sci. Eng. C*, **101**, 42 (2019).
49. L. Qin, L. Feng, C. Li, Z. Fan, G. Zhang, C. Shen and Q. Meng, *J. Clean. Prod.*, **228**, 112 (2019).
50. A. S. Mohammadi and M. Sardar, *J. Health Environ.*, **5**(4), 497 (2013).